Advanced Materials Design Group amdg.science

Cross Polarization for Improved Digital Image Correlation

LePage W, Daly SH, Shaw JA

PUBLISHED AS

LePage W, Daly SH, Shaw JA. “Cross Polarization for Improved Digital Image Correlation.” Experimental Mechanics 56, 969-985 (2016).

https://doi.org/10.1007/s11340-016-0129-2

This version of the article has been accepted for publication, after peer review (when applicable) and is subject to Springer Nature’s AM terms of use, but is not the Version of Record and does not reflect post-acceptance improvements, or any corrections. The Version of Record is available online at:
https://doi.org/10.1007/s11340-016-0129-2

Self-archived by the authors in accordance with the publisher’s self-archiving policy. Provided for educational and personal use. Please cite the version of record.

ACCEPTED MANUSCRIPT · SELF-ARCHIVED AUTHOR VERSION

Cross Polarization for Improved Digital Image Correlation

William S. LePage[*], Samantha H. Daly[†], and John A. Shaw[‡]

Abstract

Digital image correlation (DIC) is a surface deformation measurement technique for which accuracy and precision are sensitive to image quality. This work presents cross polarization, the use of orthogonal linear polarizers on light source(s) and camera(s), as an effective method for improving optical DIC measurements. The benefits of cross polarization are characterized through quantitative and statistical comparisons from two experiments: rigid body translation of a flat sample and uniaxial tension of a superelastic shape-memory alloy (SMA). In both experiments, cross polarization eliminated saturated pixels that degrade DIC measurements, and increased image contrast, which enabled higher spatial precision by using smaller subsets. Subset sizes are usually optimized for correlation confidence interval (typically with subsets of 21×21 px or larger), but can be decreased to achieve the highest possible spatial precision at the expense of increased correlation confidence intervals. Smaller subset sizes (such as 9×9 px) require better images to maintain correlation within error thresholds. By comparing DIC results from a uniaxial SMA tension test with unpolarized and cross-polarized images, we show that for 9×9 px subsets, the loss of valid DIC data points was reduced almost ten-fold with cross polarization. The only disadvantage we see to cross polarization is the decrease in specimen illumination due to transmission losses through the polarizers, which can easily be accommodated with sufficiently intense light sources. With the installation of relatively inexpensive linear polarizing filters, an optimum optical DIC setup can provide even better DIC measurements by delivering images without saturated pixels and with higher contrast for increased DIC spatial precision.

Keywords: digital image correlation; DIC; cross polarization; optical imaging

[*]Department of Mechanical Engineering, University of Michigan, Ann Arbor, MI 48109, USA

[†]Departments of Mechanical Engineering/Materials Science & Engineering, University of Michigan, Ann Arbor, MI 48109, USA

[‡]Corresponding Author, jashaw@umich.edu, Department of Aerospace Engineering, University of Michigan, Ann Arbor, MI 48109, USA

1 Introduction

Digital image correlation (DIC) is a surface displacement and deformation measurement technique that was pioneered in the 1980s [1, 2] and has become a popular method in experimental mechanics. It provides capabilities beyond the averaged, discrete measurements provided by traditional strain gages and extensometers. DIC is a non-contact, optical method that measures nonuniform displacement fields, providing quantitative measurements of heterogeneous material deformations arising from features such as stress concentrations, sites of damage accumulation, and localized phase transformations. DIC is normally limited to measuring surface displacements, but the principles of DIC have been extended to digital volume correlation (DVC) for measuring internal displacements with through-thickness imaging methods such as x-ray tomography [3] and confocal microscopy [4]. In this work, we will address improvements to macroscopic, optical, surface DIC measurements.

The basic DIC procedure consists of (1) applying a speckle pattern to the surface of a specimen, (2) taking a sequence of grayscale digital images of the specimen during a mechanical experiment, and (3) performing DIC analysis, usually as a post-processing step (since it is computationally intensive) to calculate displacements and strains of the specimen surface. Thus, good measurements require high-quality speckle patterning and high-quality images.

1. The attributes of optimum speckle patterns include a non-repeating pattern of dots (speckles), high grayscale contrast, and speckle diameters of at least 3 px to avoid aliasing [5, 6], but still small enough to maintain desired spatial precision [7]. Good patterning to obtain speckles of a relevant size and random distribution is an art, usually applied for macroscopic testing by airbrush painting (and by techniques such as self-assembling nanoparticles for microscale testing [8]). While important to the success of DIC, speckle patterning is not the focus of this work. Recommendations can be found in prior work [9, 10].

2. The fundamental data acquisition method of DIC is image capturing. If a single camera is used, only in-plane displacements (u, v) are obtained, so it is termed 2-D DIC. If two synchronized cameras are used, all three displacements (u, v, w) can be obtained, so it is termed 3-D DIC (or stereo DIC)[a].

3. Many DIC codes have been developed, but they use the same methodology to optimize a

[a]We have chosen "3-D DIC" to describe our DIC measurements with three dimensions of displacement. While 3-D DIC does provide all three displacements, it is still a surface measurement that only provides in-plane gradients of displacement (thus, four components of the deformation gradient, or equivalently three strain components and one rotation). It should not be confused with volumetric DIC (DVC), which can provide the full 3-D deformation gradient (nine components, or six strain components and three rotations).

cross-correlation function of grayscale intensities of the patterned surface to compute point-by-point displacements between a reference image and deformed image(s). The earliest and most common algorithms perform local DIC by discretizing the area of interest into groups of pixels called subsets [2]. Global DIC methods have also been developed [11], with a set of nodes akin to a finite element mesh instead of the subset-based methods of local DIC. We used local DIC in this work, but the same requirements for good speckle patterning and imaging apply to both methods.

Metrics on the influence of image quality for DIC analysis (step 2 above) and recommendations to achieve optimal results are presented in this work. In short, the usual best practices for good scientific photography apply here. The goals for imaging are sharp focus, good depth of field (where required), high contrast, and uniform and diffuse illumination. Sharp focus may require relatively fast exposure times to minimize noise [12] and motion blur [6], yet this requires intense lighting. The lighting should be bright enough for fast exposure times, yet should not cause saturated pixels, which prohibit sub-pixel displacement accuracy and increase correlation error [6]. Usually, optical DIC is best performed with direct line-of-sight to the specimen surface, to avoid refraction issues and aberrations from intervening optics or other transparent materials (such as environmental chamber windows), since imaging through glass can increase correlation error [13]. Other (perhaps obvious) best practices include the use of rigid camera mounts, the use of moderate lens apertures to avoid accentuated lens distortions at extreme apertures, the removal of dust from lenses and camera sensors, and the avoidance of thermal gradients that also can cause light aberrations.

This work characterizes the technique of cross polarization for optical DIC, and presents two experiments to quantify the effects of cross polarization with common cameras, lights, and speckle patterning method. Although cross polarization is an established technique for studio [14], archival [15], forensic [16], dental [17], ophthalmological [18], and dermatological [19] imaging, it is a new practice for DIC. Independently and simultaneously, the group of Cooper, Skaggs, and Reu, and the group of LePage, Shaw, and Daly introduced cross polarization for DIC experiments [20, 21]. When light illuminates a specimen, reflections can be roughly classified into two types, specular reflections[b] (from smooth areas of the surface) that preserve their light polarity and diffuse reflections (from rough areas of the surface) that do not. Specular reflections appear to the camera as high intensity (shiny) spots on the surface and can lead to pixel saturation (glare). From rougher areas of the surface, however, light intensity is diminished and light polarity is strewed when

[b]The terminology is unfortunate in this context. In the optics community, "specular" reflections are defined as those reflections that maintain their polarity. This should not be confused with the "speckle" DIC pattern, which is defined as a random (non-periodic), black-white pattern of dots.

scattered from asperities and sub-surface scattering centers (Figure 1a) [22]. With flat samples, specular reflections can be minimized by placing the lights and cameras in positions that avoid direct reflections (which have equal angles for incident and transmitted light rays) from the sample surface. This is not possible with rounded samples such as tubes and cylinders, however. Thus, the benefits of cross polarization described in this paper are likely even greater for round samples than for the flat samples presented here. The technique of cross polarization simply consists of placing a linear polarizer between the light source and the specimen and a second polarizer (of a perpendicular polarization axis to the first one) between the specimen and the camera. Thus, the orthogonal polarization between incident and reflected light off the specimen surface selectively attenuates just the specular reflections, resulting in diffuse lighting to the camera (Figure 1b).

2 Rigid body translation experiment

First, a comparison between unpolarized and cross-polarized imaging for macroscopic optical DIC is presented with 2-D DIC and 3-D DIC setups simultaneously capturing precise rigid body

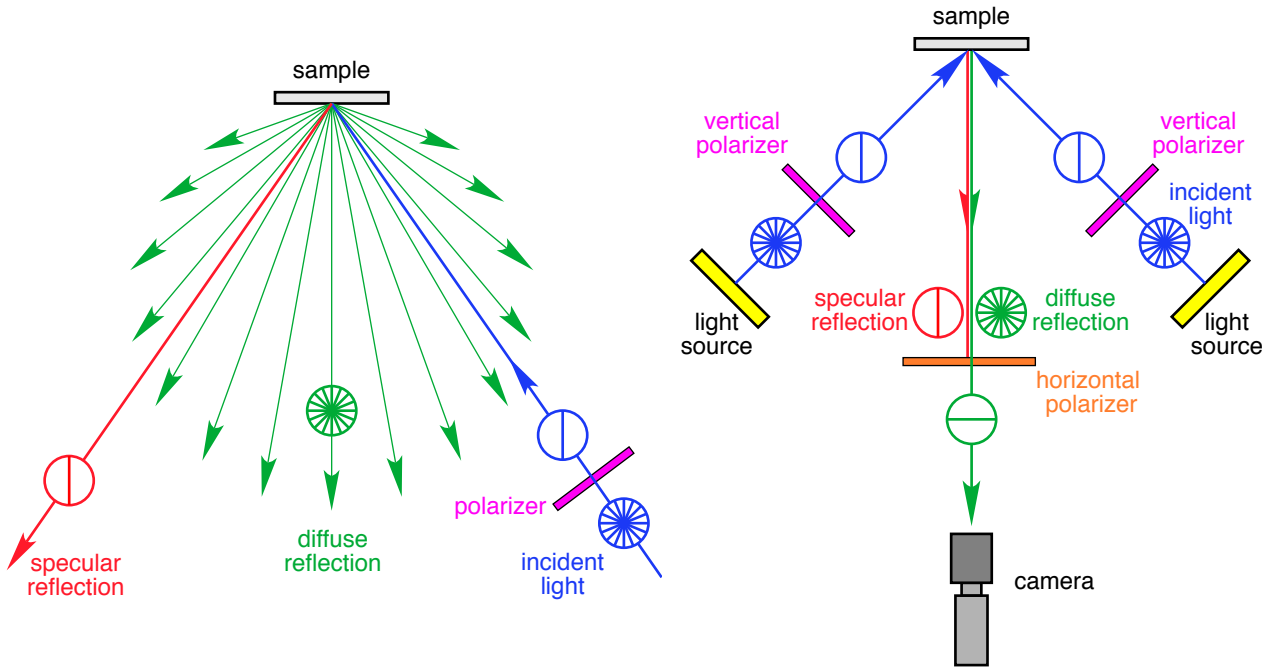

(a) Specular and diffuse reflections

(b) Cross polarization

Figure 1: (a) Specular reflections maintain the polarization of incident light, while diffuse reflections do not. (b) The horizontal polarizer on the camera's lens attenuates the vertically polarized specular reflections to avoid saturated pixels.

translations of a sample with different speckle patterns.

2.1 Speckle patterning

Four different speckle patterns were prepared on a single sample to compare unpolarized versus cross-polarized images. A thin base coat of white paint (Golden High Flow Titanium White, no. 8549-4, lot 366162) was sprayed on a 50 mm × 50 mm area of an unfinished aluminum sheet (80 mm × 80 mm × 0.4 mm thick) with an airbrush (Iwata CM-B with 0.18 mm fluid nozzle and needle, and Iwata Studio Power Jet air compressor) at 210 kPa (30 psi) until all of the aluminum in the painted area was just covered. This was done to avoid glare from the aluminum [23], and complete coverage was verified under a stereo microscope (Olympus BX51M stereo microscope in bright field with 5× magnification MPLN objective lens). Speckle patterns were applied by airbrush with a 1:1 mixture of methanol and black paint (Golden High Flow Carbon Black, no. 8040-4, lot 345307). Methanol is added to the black paint to decrease viscosity and maintain good paint flow and consistent speckle sizes at low airbrush pressures. To create four patterns of different speckle sizes, a different airbrush pressure was used in each of the four 25 mm × 25 mm quadrants of the white-painted area, while masking the other three quadrants (Figures 2 and 4). The quadrants are labelled I, II, III, IV, respectively, in order of increasing pressure 70, 140, 175, and 420 kPa (10, 20, 25, 60 psi), corresponding to decreasing speckle size. The best speckle patterns have speckles larger than 3 px (as imaged with the DIC setup) to avoid aliasing [5, 6], but not much larger so that DIC data resolution is maximized [7]. Here, quadrant I represents acceptable speckle size, while patterns III and IV have undersized speckles. The undersized speckle patterns are included to assess the efficacy of cross polarization for imaging sub-optimal speckle patterns.

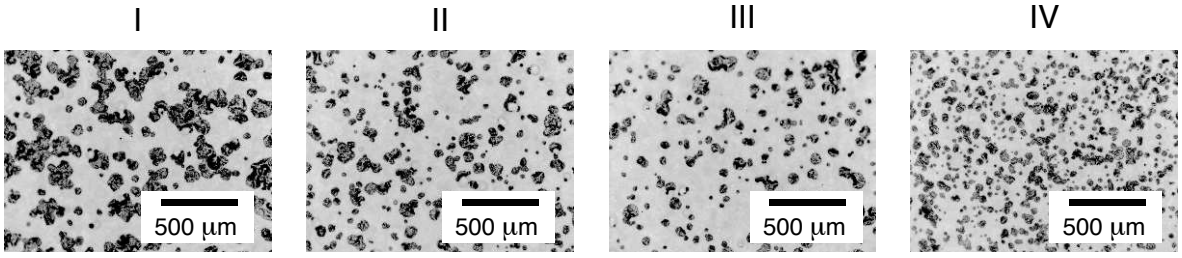

Figure 2: Light microscope images showing the four quadrants (I, II, III, and IV) with progressively increasing airbrush pressures (70 kPa, 140 kPa, 175 kPa, and 420 kPa, respectively) and consequent decreasing speckle sizes. Quadrant I has acceptable speckle size when imaged with the DIC cameras, with the exception of some undersized speckles, while the other quadrants, especially III and IV, have undersized speckles to characterize unpolarized versus cross-polarized conditions for sub-optimal speckle patterns.

2.2 Imaging setup

The painted aluminum sample was placed in a linear translation stage, driven by a motorized actuator (Newport TRB25CC) with 0.1 μm minimum increment of motion, 1.5 ± 0.2 μm bi-directional repeatability from backlash, and 25 mm range of motion. The actuator speed was kept slow (0.2 mm/s, 10% of maximum actuator speed) for all translations, and images were captured when the actuator was stopped. Three CCD cameras (Point Grey GRAS 50S5M-C) were positioned 0.8 m from the sample, as shown in Figure 3. Cameras 1 and 3 were used for 3-D DIC with an included angle of 11^{o} between them, and Camera 2 was positioned between the other two oriented perpendicular to the sample for 2-D DIC. The three cameras simultaneously captured images of the aluminum sample with an aperture of f/8 and 25 ms exposure. Cameras 1 and 3 had 75 mm Fujinon HF75SA-1 lenses, while Camera 2 had a 50 mm Fujinon HF50SA-1 lens. Two LED light panels (LitePanels no. 903-2076, each with 40W power, or 500W tungsten equivalent, and 1,537 lux at 1.2 m) were placed at 0.3 m from the sample, oriented at ±45^{o} to provide primary lighting. For the cross-polarized case, linear polarizing PMMA films (American Polarizers, Inc., AP38-030T with 38% transmission) were installed on both light panels in a vertical polarizing direction, and linear polarizing glass filters (Edmund Optics #36-440 with 30% transmission) were installed on all three camera lenses in a horizontal polarizing direction. For the unpolarized case, all polarizing films and filters were removed. Prior to each experiment, the brightness of the light panels was increased just until no saturated pixels were observed in the painted area of the sample. The light panel power knobs were set to about 60% without polarization and 90% with cross polarization to accommodate light transmission losses. Note that the panel power setting changes the light intensity output nonlinearly, so this increase in lighting is about two to three f-stops, or a four-fold to eight-fold increase of the light intensity.

2.3 DIC calibration

The 2-D DIC length scale was calibrated with the known distance between corners A and C of the sample's painted area (see Figure 4a). The 2-D length scale calibration was measured on the sample with calipers and pinpointed in the images to ±1 px on each endpoint. The paired cameras (1 and 3) were calibrated for 3-D DIC with a laser-printed calibration grid (via Correlated Solutions Calibration Grid Generator software, with 6 mm spacing). The same calibration score (0.059 px residual) was achieved for all 10 trials by selecting among about 25 calibration images.

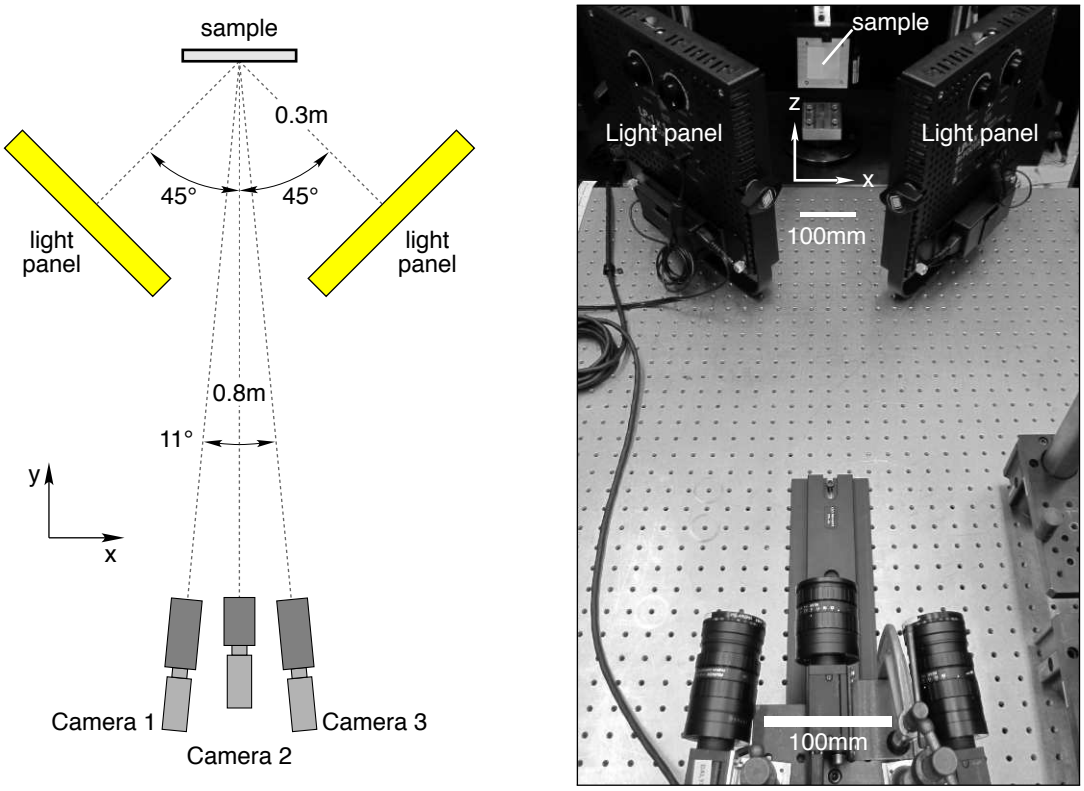

(a) Top view schematic

(b) Photograph of setup

Figure 3: Schematic (a) and photograph (b) of the rigid translation experimental setup, with two LED light panels illuminating the sample and three cameras simultaneously capturing images for 2-D DIC and 3-D DIC. The sample was translated upward (z-direction) incrementally to measure known w displacements.

2.4 Procedure

First, the actuator was translated downward to $w = -2.5$ mm, then upward to $w = -1.25$ mm, and upward again to $w = 0$ mm to mitigate any backlash. Reference images were captured with the actuator at $w = 0$, then eight 2.5 mm upward rigid body translations were performed, each followed by an image capture while the actuator was stopped. Five trials were performed for each of the two cases (no polarization and cross polarization), alternating between cases to avoid uneven temporal errors, due to effects such as CCD heating [6]. For each trial, all three lenses were refocused on the center of the sample and the 3-D DIC camera system was recalibrated to the same calibration score. This yielded a total of 80 translated image pairs for 3-D DIC and 80 single images for 2-D DIC.

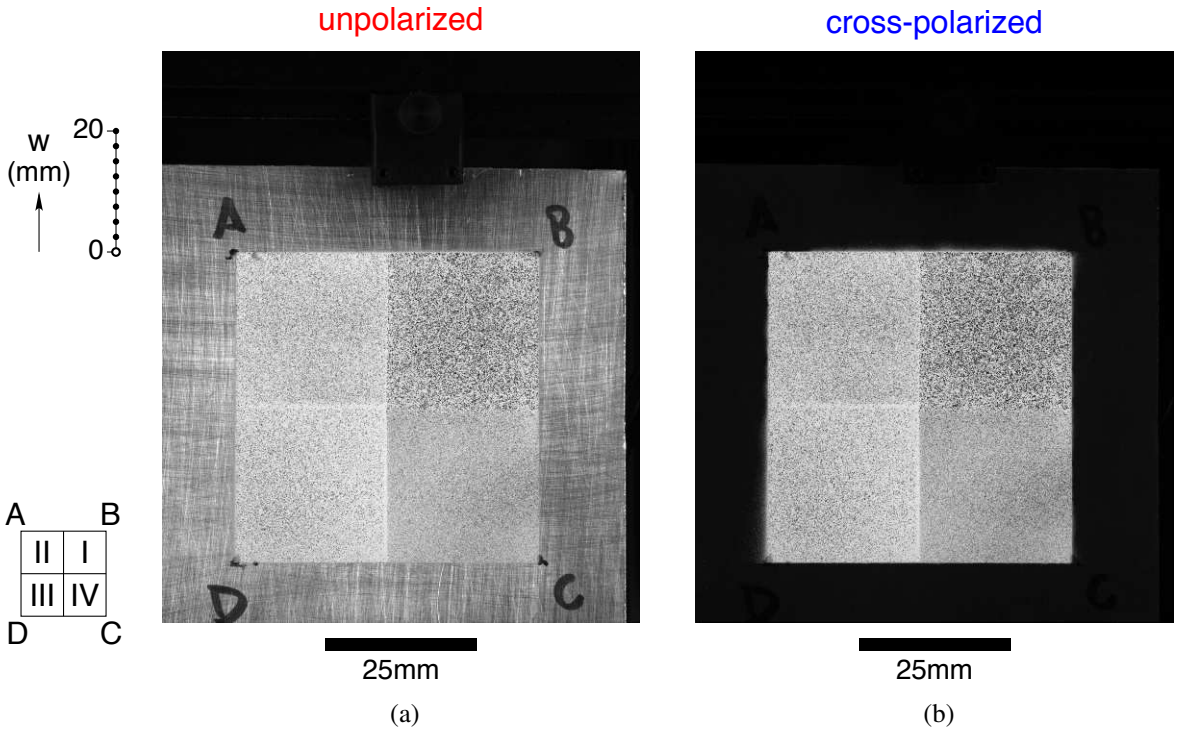

Figure 4: A comparison of full images of the sample, (a) without polarization and (b) cross-polarized, shows that specular reflections are attenuated by cross polarization. This is especially evident for the bare metal, but is also true for the speckle painted area (although less obvious to the naked eye). Both images were taken at the reference position $w = 0$ (indicated by the open circle on the vertical axis) by Camera 1 with total field of view of 80 mm wide $\times$ 95 mm tall (2048 $\times$ 2448 px). The sample was translated upward in eight 2.5 mm increments (black dots on the axis) to a final position $w_{\max} = 20$ mm, capturing a sequence of nine images, to assess the effects of distortion as speckle patterns moved away from the center of the field of view.

2.5 DIC post-processing

Correlations were performed on the four speckle pattern quadrants, representing different speckle sizes, distributions, and contrasts. The 2-D DIC and 3-D DIC analyses were performed with Vic-2D 2009 and Vic-3D 7, respectively, from Correlated Solutions. The images were first low-pass filtered (with the software's built-in tool) to reduce possible bias errors from aliasing. The images were then correlated using normalized squared differences with Gaussian subset weights and an optimized eight-tap interpolation filter for minimizing bias [6]. Correlation threshold values were 0.02 px consistency threshold, 0.05 px maximum confidence interval, and 0.1 px matchability threshold. Correlation step size (the spacing among DIC data points) was 7 px for all cases,

yielding about 2,000 2-D DIC data points and 5,000 3-D DIC data points for each 25 mm × 25 mm speckle pattern quadrant.

For all four speckle patterns and for both 2-D DIC and 3-D DIC, optimum subset sizes $m \times m$ (px) were consistently smaller for the cross-polarized cases than for their unpolarized counterparts (Figure 5). Subset sizes were chosen to optimize the correlation confidence interval (CCI) to 0.01 px for an assumed camera noise level of 8, using the built-in subset size selection tool within the Correlated Solutions software. Average values and spreads for each set of five trials are shown in Figure 5. In this (Figure 5) and subsequent figures (Figures 7–9), open (red) and closed (blue) circles denote mean values for unpolarized and cross-polarized cases, respectively, the error bars bound about ±2.7 standard deviations, and outliers are shown by small black dots. Cross polarization always resulted in a reduction in the average optimum subset size and usually resulted in less variability (all but one case, which was about the same). Smaller subset sizes are generally desirable, since they have less spatial smoothing from their smaller shape functions.

To enable a consistent comparison between unpolarized and cross-polarized results below, however, the same (intermediate) subset size was chosen (Table 1) for each speckle pattern and 2-D or 3-D DIC calculation. DIC displacements were computed with 2-D DIC (u, w) and 3-D DIC (u, v, w) and compared pointwise to the actuator translations (w_0) to quantify the magnitude

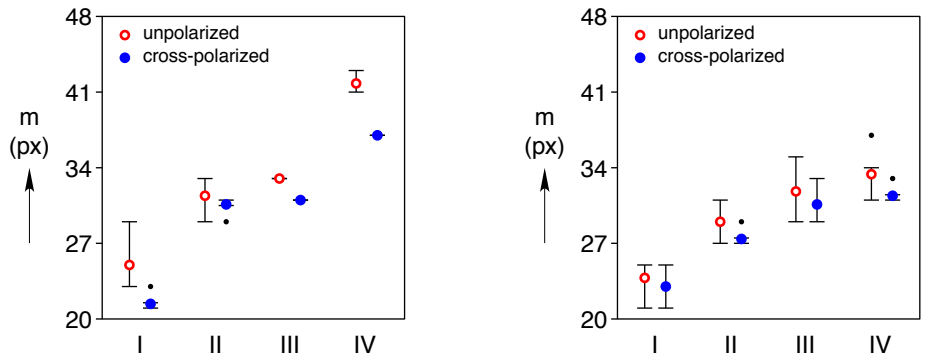

(a) 2-D DIC (b) 3-D DIC

Figure 5: Mean values for optimum subset sizes $m \times m$ (px) with cross polarization (blue, closed circles) were consistently smaller than without polarization (red, open circles) in all cases: four speckle patterns I, II, III, IV and using 2-D DIC or 3-D DIC. The error bars (about ±2.7 standard deviations) also generally show reduced variability of the optimum subset size with cross polarization.

	Optimum subset size (px) for each speckle pattern			
Quadrant	I	II	III	IV
2-D DIC	23	31	33	39
3-D DIC	23	29	31	33

Table 1: Fixed DIC subset sizes were chosen to provide consistent comparisons (Figures 8–10 below) between unpolarized and cross-polarized cases. Each subset size is a selected intermediate value of the optimum values shown in Figure 5.

of respective displacement errors, according to

$$\Delta w_{2D} = \left| \sqrt{u^2 + w^2} - w_0 \right|, \tag{1a}$$

$$\Delta w_{3D} = \left| \sqrt{u^2 + v^2 + w^2} - w_0 \right|. \tag{1b}$$

The pointwise errors Δw_{2D} and Δw_{3D} were averaged across each quadrant to obtain four values of $\overline{\Delta w}_{2D}$ and $\overline{\Delta w}_{3D}$ for each image.

2.6 Results from rigid body translation experiment

Cross polarization reduces or eliminates saturated pixels, which are undesirable because saturated pixels prohibit sub-pixel accuracy and increase correlation error [6]. The appearance of saturated pixels during optical DIC experiments is difficult to avoid, as lighting conditions effectively change with large translations and deformations, despite fixed light positions and settings. In the experiments presented here, the light panel brightness was increased just until no saturated pixels were observed in the DIC area of interest in a live view of the cameras. After translations of the sample, however, saturated pixels appeared in most of the unpolarized trials, while no pixels were saturated for any cross-polarized cases (Table 2). One should recognize that the changes in illumination here are relatively mild for such a simple rigid body translation, and we would expect much larger issues for "real-world" experiments involving out-of-plane displacements and/or curved specimen surfaces (such as column buckling of a cylindrical rod). Thus, the protection that cross polarization provides against saturated pixels makes DIC measurements significantly more robust.

In addition to minimizing saturated pixels, cross polarization improves image contrast, which reduces DIC correlation error by increasing intensity gradients [12]. Figure 6 provides two examples of speckle patterns, Quadrant I (Figure 6a) and Quadrant III (Figure 6b) both taken by Camera 1, to compare unpolarized and cross-polarized images. The corresponding histograms

	Total saturated pixel count			
	2-D DIC (Camera 2)		3-D DIC (Camera 1)	
Quadrant	unpolarized	cross-polarized	unpolarized	cross-polarized
I	0	0	36	0
II	31	0	77	0
III	324	0	2965	0
IV	0	0	1	0

Table 2: During the rigid body translation experiments, saturated pixels appear in most of the unpolarized trials, despite setting the initial lighting to have no saturated pixels in the reference position ($w = 0$). By contrast, no saturated pixels appear for any of the cross-polarized trials.

(Figures 6c and 6d, respectively) were accumulated across all 10 trials, giving the total pixel count (N) at each grayscale value within the 8-bit (256) dynamic range of the CCD sensor. Quadrant I represents a good speckle pattern with a broad distribution of grayscale values, while Quadrant III represents a pattern with undersized speckles as evident from its relatively narrow distribution of grayscale values. Overall, cross polarization darkened both sets of images, which is apparent both to the eye and by the left-shift of the histograms to darker (smaller) grayscale values. The improvement in contrast from cross polarization is less obvious to the eye, but can be seen in the histograms by the slight broadening of each distribution. For Quadrant I, the contrast increased by 6 grayscale counts for 3-D DIC (Figure 6c), which might appear to be only a modest improvement, but we consider it an appreciable gain since the unpolarized case already had an optimum speckle pattern and lighting condition. For Quadrant III with finer speckles, cross polarization resulted in a contrast gain of 2 grayscale counts, which is still significant considering the narrow histogram distribution. Relative to the nominal width of each unpolarized distribution (200 and 76, respectively), cross polarization gives about a 3% gain in contrast, even under excellent lighting conditions. We expect larger improvements would be achieved under less optimal lighting, especially over-bright lighting conditions[c]. Furthermore, although not shown here explicitly but still relevant for undersized speckles (like Quadrant III), cross polarization removes any small spots of glare (even black speckles can be smooth and reflective), thereby minimizing the blooming effect[d] of white paint around small spots of black paint (Figure 6).

Of course, to achieve this increase in contrast, sufficiently bright lights must be used, so that the cross-polarized setup can have the same aperture and exposure time (camera gain) as the unpo-

[c]Of course, cross polarization could adversely affect an under-illuminated setup, but that is easily avoided.

[d]Blooming occurs in imaging when fringes extend beyond a bright feature into a dark feature.

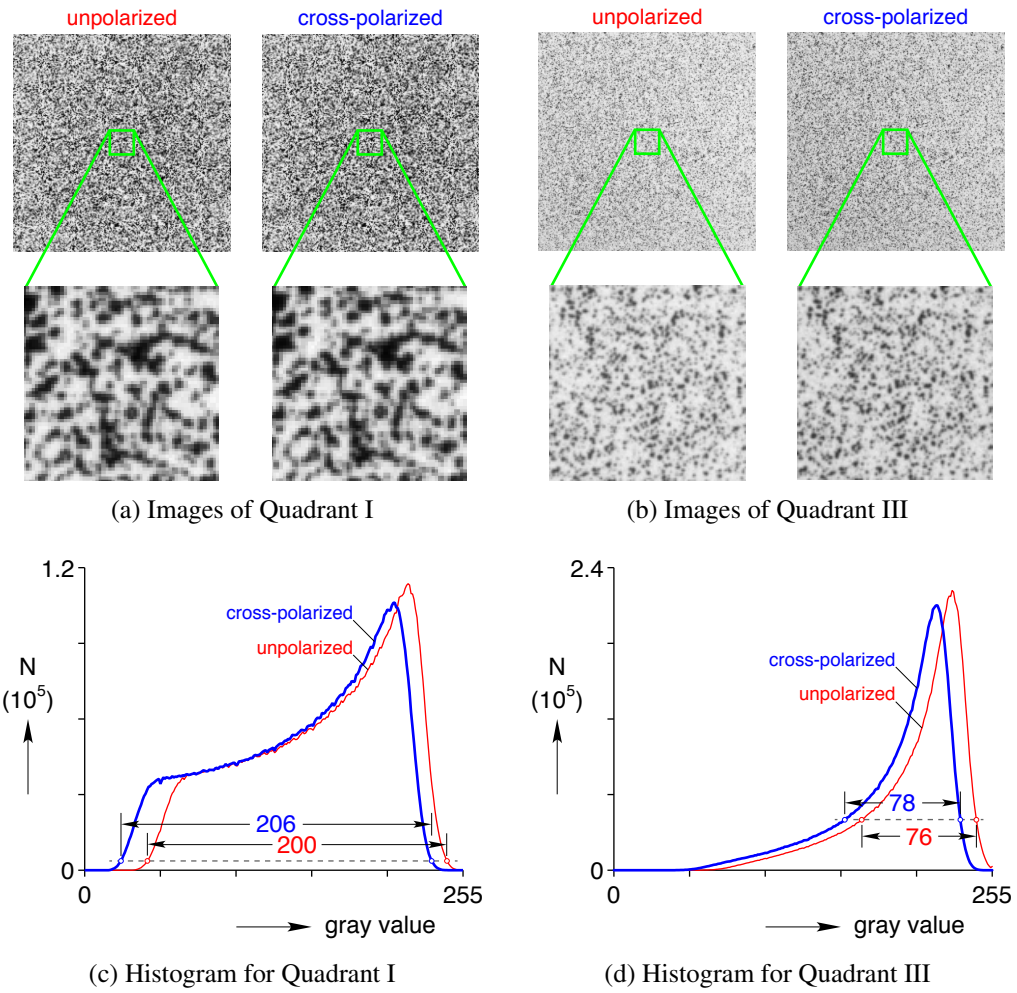

(a) Images of Quadrant I

(b) Images of Quadrant III

(c) Histogram for Quadrant I

(d) Histogram for Quadrant III

Figure 6: A comparison of images and histograms of two speckle patterns (Quadrants I and III) shows that cross polarization results in about a 3% gain in contrast (6 and 2 grayscale counts, respectively) relative to the nominal distribution width. Images (a) and (b) were taken by Camera 1, and their corresponding histograms (c) and (d) give the total pixel count (N) at each of the 256 grayscale values accumulated over all 10 trials.

larized setup. If the brightness was not adjusted, then light transmission losses from the polarizers would decrease the available light intensity by a factor of about 8. This is why the light source power was increased for the cross-polarized cases, which allowed all images here (whether polarized or not) to be captured at f/8 with a fixed exposure time.

Consistent with the increased contrast, cross polarization also increases the mean intensity gradient (Figure 7), which has been proposed as a metric to evaluate DIC speckle pattern quality [24]. The mean intensity gradient ($\overline{\nabla G}$) was computed for each image, (taken by Camera 2 for 2-D DIC

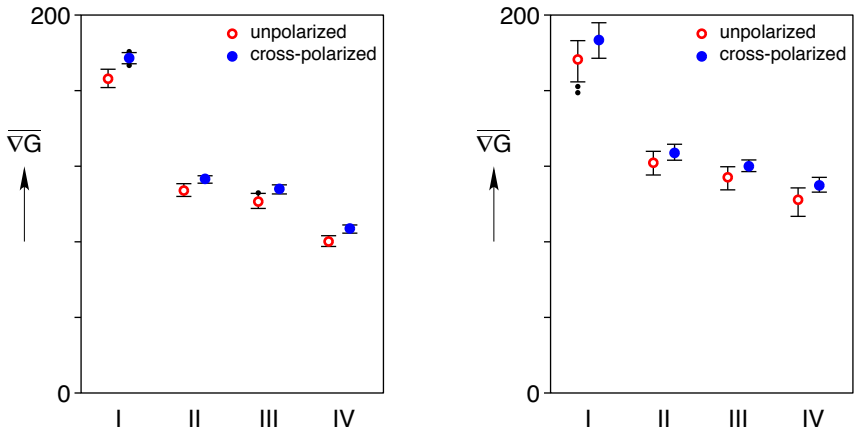

(a) 2-D DIC (b) 3-D DIC

Figure 7: Cross polarization increased the mean intensity gradient ($\overline{\nabla G}$) on average by about 7% for 2-D DIC and 6% for 3-D DIC. A large mean intensity gradient indicates high-quality speckle pattern, lighting, and images. Each data set (mean with about ±2.7 standard deviation error bars) contains 40 data points.

and Camera 1 for 3-D DIC) using

$$\overline{\nabla G} = \frac{\sum_{i=1}^{W} \sum_{j=1}^{H} \left|\nabla f(\boldsymbol{x}_{ij})\right|}{WH}, \tag{2}$$

where W and H are the DIC area of interest width and height in pixels, $|\nabla f(\boldsymbol{x}_{ij})| = \sqrt{(f_{,x})^2 + (f_{,y})^2}$ is the magnitude of the local intensity gradient vector, and $f_{,x}$ and $f_{,y}$ are the in-plane derivatives at pixel $\boldsymbol{x}_{ij}$. $\overline{\nabla G}$ was calculated by the Prewitt filter, an approximate differential operator for the intensity gradient [25].

Cross polarization reduced the correlation confidence interval (CCI) by at least 5.2% and 6.3% for 2-D and 3-D DIC, respectively (Figure 8). The CCI is a statistical measure of the one standard deviation confidence region for each subset, where a smaller CCI indicates better correlation accuracy. Cross polarization decreased the mean CCI for 3-D DIC, for example, by 7.8%, 6.3%, 6.4%, and 8.1% for speckle quadrants I, II, III, and IV, respectively. A summary of the resulting measurement errors are provided in Figure 9. As shown in Figure 9a for 2-D DIC, significant reductions in mean measurement error (56%, 52%, 55%, and 61%) were obtained for all speckle patterns (I, II, III, and IV, respectively). Interestingly, no appreciable reductions in displacement measurement error were observed with 3-D DIC (Figure 9b) by using cross polarization, probably since the errors were already quite small.

More details of the displacement errors (Δw) and CCIs, plotted against the normalized (aver-

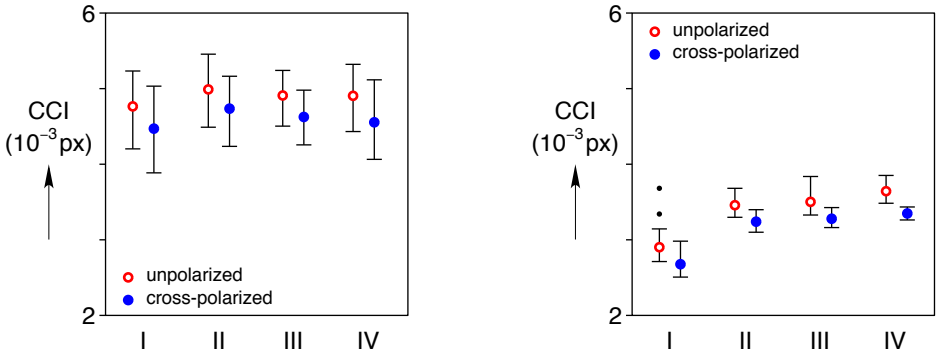

(a) 2-D DIC (b) 3-D DIC

Figure 8: Cross polarization consistently provided reductions in the correlation confidence interval (CCI), where a smaller CCI indicates better correlation. Each data set (mean with about ±2.7 standard deviation error bars and dot outliers) contains 40 data points.

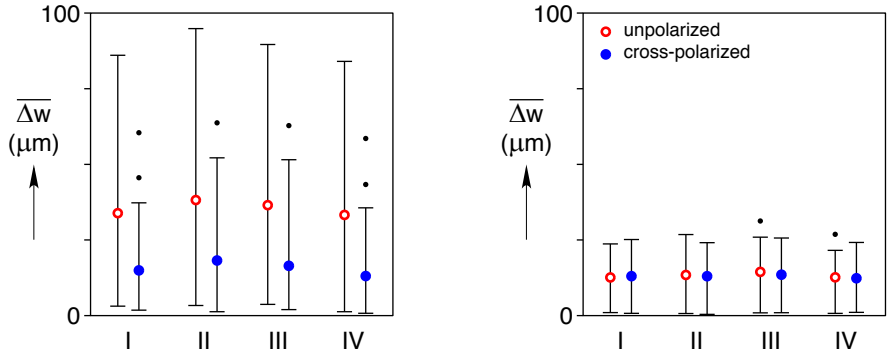

(a) 2-D DIC (b) 3-D DIC

Figure 9: For 2-D DIC, significant reductions (56%, 52%, 55%, and 61%) in the mean measurement error were observed for speckle patterns I, II, III, and IV, respectively, by using cross polarization versus no polarization. No significant reduction in displacement measurement error was observed for 3-D DIC by using cross polarization, probably because the unpolarized condition was already optimized for minimum specular reflections by placing the cameras outside of the direct reflections of the light panels. Each data set (mean with about ±2.7 standard deviation error bars) contains 40 data points.

age) rigid translation $\overline{w}/H$, are provided in Figure 10 to gain a sense of where (and where not) cross polarization provides an improvement. For 2-D DIC (Figure 10a), cross polarization on average achieved a 48% lower mean error. Errors were reduced at all displacements, but it made the largest error reductions at the largest displacements. The CCI for 2-D DIC (Figure 10b) exhibited a non-monotonic change with displacement, with a local minimum near $\overline{w}/H \approx 12\%$ as the sam-

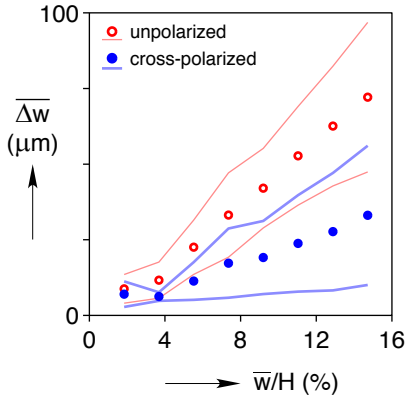

(a) 2-D DIC displacement error

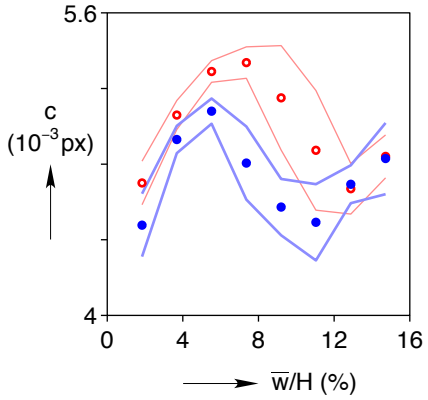

(b) 2-D DIC correlation confidence interval

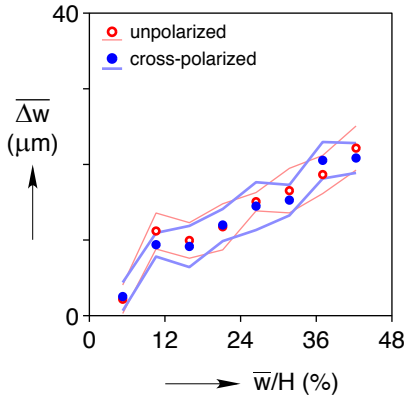

(c) 3-D DIC displacement error

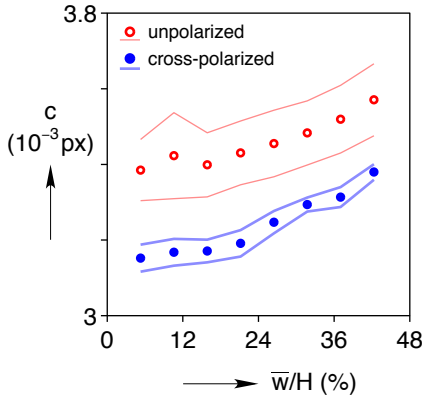

(d) 3-D DIC correlation confidence interval

Figure 10: Measurement errors (Δw) and correlation confidence intervals (CCI) are plotted against the normalized average displacement $\overline{w}/H$ (where H is the field of view height) to show where cross polarization provided improvement. Circles denote mean values for all four speckle quadrants across all five trials of each polarization, and the lines correspond to ± 1 standard deviation from the mean values.

ple translated through the center of the field of view where lens distortions were lowest. For all but one displacement value, cross polarization gave a smaller CCI than without polarization. For 3-D DIC (Figure 10c), no appreciable reduction in displacement error was observed, consistent with Figure 9b. Cross polarization, however, consistently achieved lower average CCIs across all displacements (Figure 10d), indicating better DIC measurements.

3 Uniaxial tension experiment

To illustrate the differences between cross-polarized and unpolarized images in a less trivial context with a deforming specimen, a superelastic nickel-titanium (NiTi) specimen was loaded in uniaxial tension. NiTi was chosen for its large recoverable strains, localized phase transformations, and the repeatable pattern of stress-induced martensitic (SIM) phase transformation upon cycling [26]. During tension experiments, these properties result in distinctly nonuniform deformations and allow reasonably congruent comparisons between cycles with different polarization conditions while using the same cameras and lenses.

3.1 Uniaxial specimen

The specimen was the same material and dimensions as those from previously published experiments [26, 27]. The test specimen was cut from a flat, 0.281 mm thick sheet of superelastic NiTi, with the rolling direction parallel to the loading z-axis, by wire EDM to the dimensions shown in Figure 11a. The front surface of the specimen was patterned with a white base coat at an airbrush pressure of 210 kPa (30 psi) followed by black speckles at 70 kPa (10 psi), using the same equipment reported in Section 2.1. A closeup optical micrograph of the speckle pattern is provided in Figure 11b.

3.2 Experimental setup

In this setup all measurements were taken using 3-D DIC. Cameras 1 and 3 were outfitted with 20 mm extension tubes to give an appropriate field of view and were oriented with an included

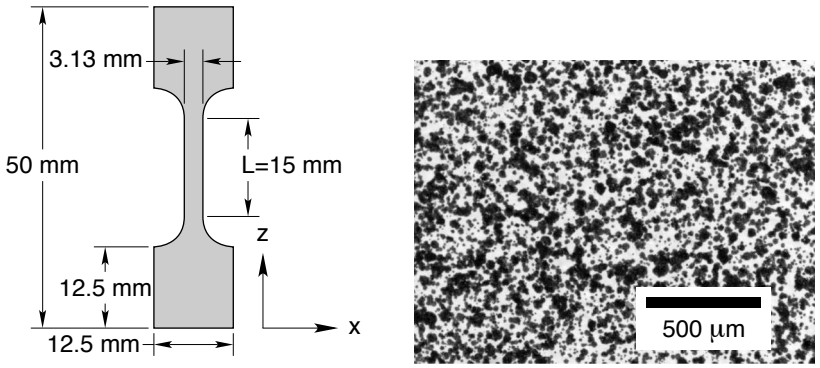

Figure 11: (a) Schematic of the tension specimen, (b) micrograph of the speckle pattern.

angle between them of 8°, balancing depth of focus while still capturing out-of-plane displacements. All images for the uniaxial tension experiments (about 110 images per load-unload cycle) were captured at an aperture of f/5.6 and a 15.0 ms exposure time. The 3-D DIC system was calibrated with a glass calibration grid (Applied Image p/n 045466, grid A, with 1.780 mm spacing). Between changes to polarization conditions, the lenses were refocused, the sample was removed from the grips, the system was recalibrated to a constant calibration score of 0.036 px residual, and the sample was placed back in the same position in the grips. The same LED light panels as before were used, with brightnesses of about 60% and 90% for unpolarized and cross-polarized imaging, respectively. The specimen was loaded slowly in displacement (δ) control by a TestResources model 830 load frame at constant ramp rates $\dot{\delta} = \pm 0.0024$ mm/s, or $\dot{\delta}/L = \pm 1.92 \times 10^{-4} \mathrm{s}^{-1}$ across the gage section. The axial load resultant P was measured by an MTS model 661.11 (500 N) force transducer. The data presented here for the unpolarized and cross-polarized lighting conditions were captured during loading cycles 4 and 5, respectively, on the same specimen. Figure 12 shows the engineering stress-strain response of the specimen for these two cycles, where A_0 and L are the reference cross-sectional area and reference length, respectively, of the specimen's central gage section, and δ/L is strain from a DIC virtual extensometer along the gage length L. DIC results are reported later at two points, ① and ②, on the upper plateau of the mechanical response during stress-induced, phase-transformation front propagation.

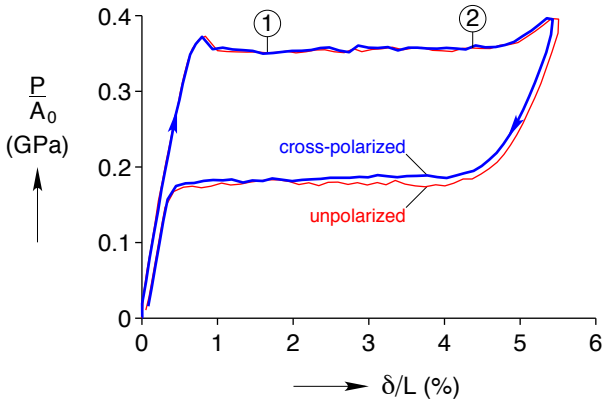

Figure 12: Mechanical response of the superelastic NiTi specimen loaded in uniaxial tension and imaged with no polarization and cross polarization during cycles 4 and 5, respectively. DIC results are presented below at ① and ② on the upper plateau of the response.

3.3 DIC post-processing

The images were correlated in Vic-3D 7 as before with low-pass filtering, Gaussian subset weights, eight-tap interpolation filter, and normalized squared differences. Correlation step sizes

were 3 px to yield about 37,000 DIC data points in the area of interest for subset sizes of 15 px. Correlation threshold values were 0.02 px consistency threshold, 0.05 px maximum confidence interval, and 0.1 px matchability threshold. Using subset size optimization to a CCI of 0.01 px and an assumed camera noise level of 8, the optimum subset sizes for unpolarized and cross-polarized conditions were 27 px and 25 px, respectively. The axial strain and the CCI fields for these optimum subset sizes are presented first in Figure 14. Next, the subset size was decreased to 15 px for both lighting conditions to decrease the spatial smoothing at the expense of increased CCI, and the resulting axial strain and CCI fields are shown respectively in Figure 15 and Figure 16. The strains were computed with a Gaussian filter size of 27 px for the 25 and 27 px optimized subsets and 15 px for the 15 px subsets.

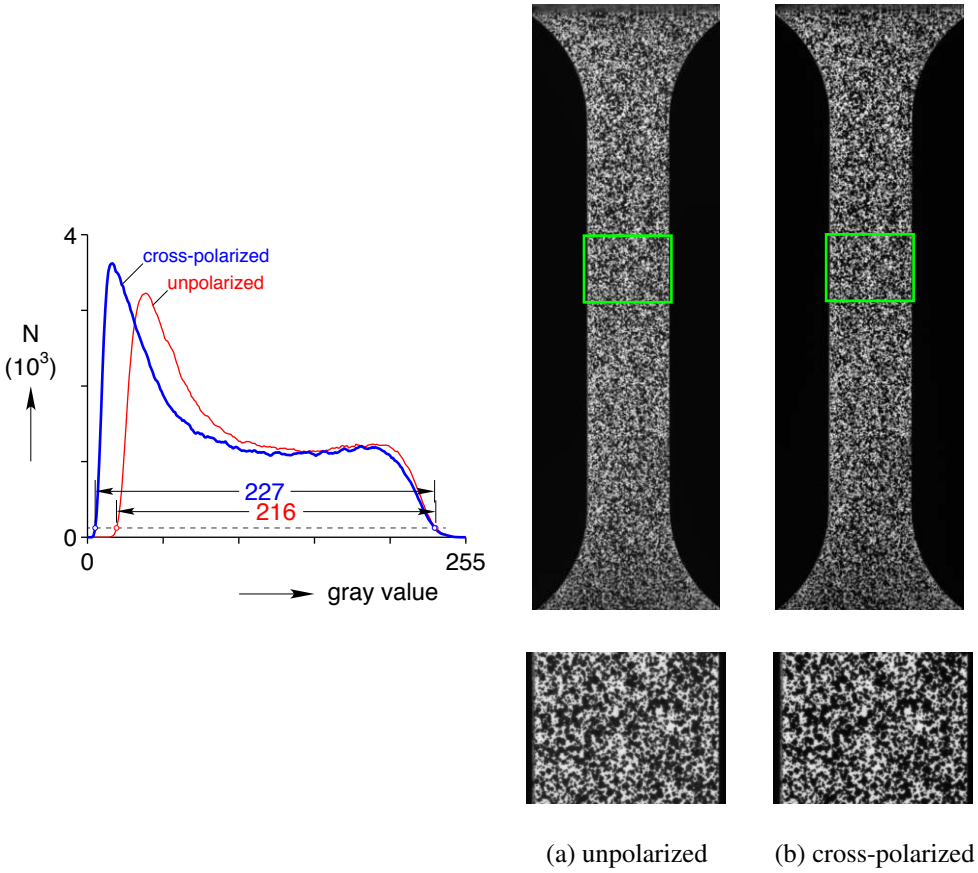

(a) unpolarized (b) cross-polarized

Figure 13: Cross polarization increased the contrast by 11 grayscale counts by darkening the black speckles in the image, as seen in the histogram produced from the pixels in the DIC area of interest of the reference image from Camera 1.

3.4 Experimental results

Similar improvements with cross polarization in contrast and mean intensity gradient were observed during the uniaxial experiment as were seen earlier in the rigid translation experiment. As shown in Figure 13, cross polarization increased the contrast in the DIC area of interest (across the gage section) by 11 grayscale counts, or 4.3% of the 8-bit sensor's dynamic range. Furthermore, cross polarization increased the mean intensity gradient by 7.4%, from 165.4 to 177.7 grayscale counts. In this experiment, cross polarization again had no saturated pixels, while only two pixels were saturated in the unpolarized images. We expect that glare was less of a problem during this experiment, since maximum displacements were on the order of 1 mm, much smaller than the 20 mm displacements for the previous rigid translation experiment, resulting in more constant lighting conditions.

With the optimum subset sizes (27 px and 25 px for unpolarized and cross-polarized images, respectively), no major differences were observed in the DIC axial strain fields (Figures 14a and 14b). The same pattern of stress-induced martensitic transformation was repeated during the two cycles, consistent with the results of Kim and Daly [26]. Cross polarization had a 2 px smaller subset size, but there was no observable difference in the spatial detail of the axial strain fields. However, cross polarization decreased the CCI by 4.6% on average, which can be seen in Figures 14c and 14d at locations of high strain gradient (across a transformation front).

Smaller subsets increase spatial precision by reducing the size of the DIC data smoothing, but at the expense of reduced confidence in the correlation. Undersized subsets cause points of lost correlation, where correlation thresholds are exceeded. If maximum spatial precision is desired more than complete continuity of data in the DIC area of interest, though, cross polarization was shown to preserve more DIC data points for very small subsets. Although no significant differences were observed with optimum subset sizes, cross polarization decreased CCIs to provide more robust correlations with small subsets. When the subset sizes were reduced to 15 px for increased spatial precision, the unpolarized images lost 1.3% of the DIC data in the area of interest (495 out of 37,459 DIC data points) due to exceeding the correlation threshold values (see the holes in the contour plots of Figures 15a and 15c). The cross-polarized images Figures 15b and 15d), however, had no lost correlation points (37,705 DIC data points). Compared to the optimum subset size CCI fields (Figures 14c and 14d), the decrease in CCI from cross polarization was also more noticeable with the smaller 15 px subsets (Figure 16). When the subset size was decreased further to 9 px (not shown), the unpolarized images lost 17.9% of the DIC data points due to exceeding the correlation error thresholds, while the cross-polarized images lost only 2.5% of the DIC data points.

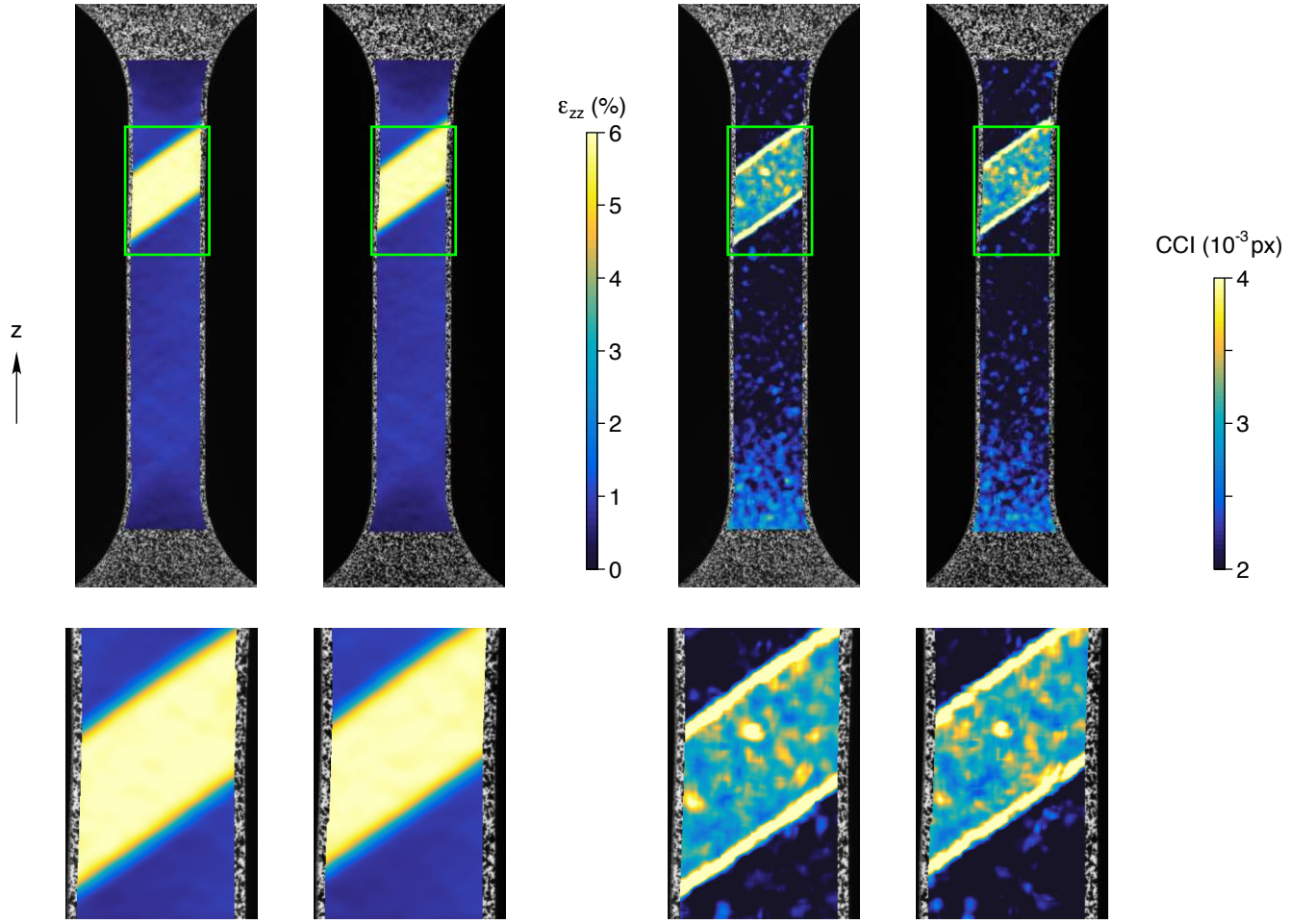

(a) Unpolarized ① (b) Cross-polarized ① (c) Unpolarized ① (d) Cross-polarized ①

Figure 14: When using optimum subset sizes (27 and 25 px, respectively), nearly identical axial strain maps were obtained between unpolarized and cross-polarized images, but cross polarization achieved slightly smaller regions of poor (large) correlation confidence intervals.

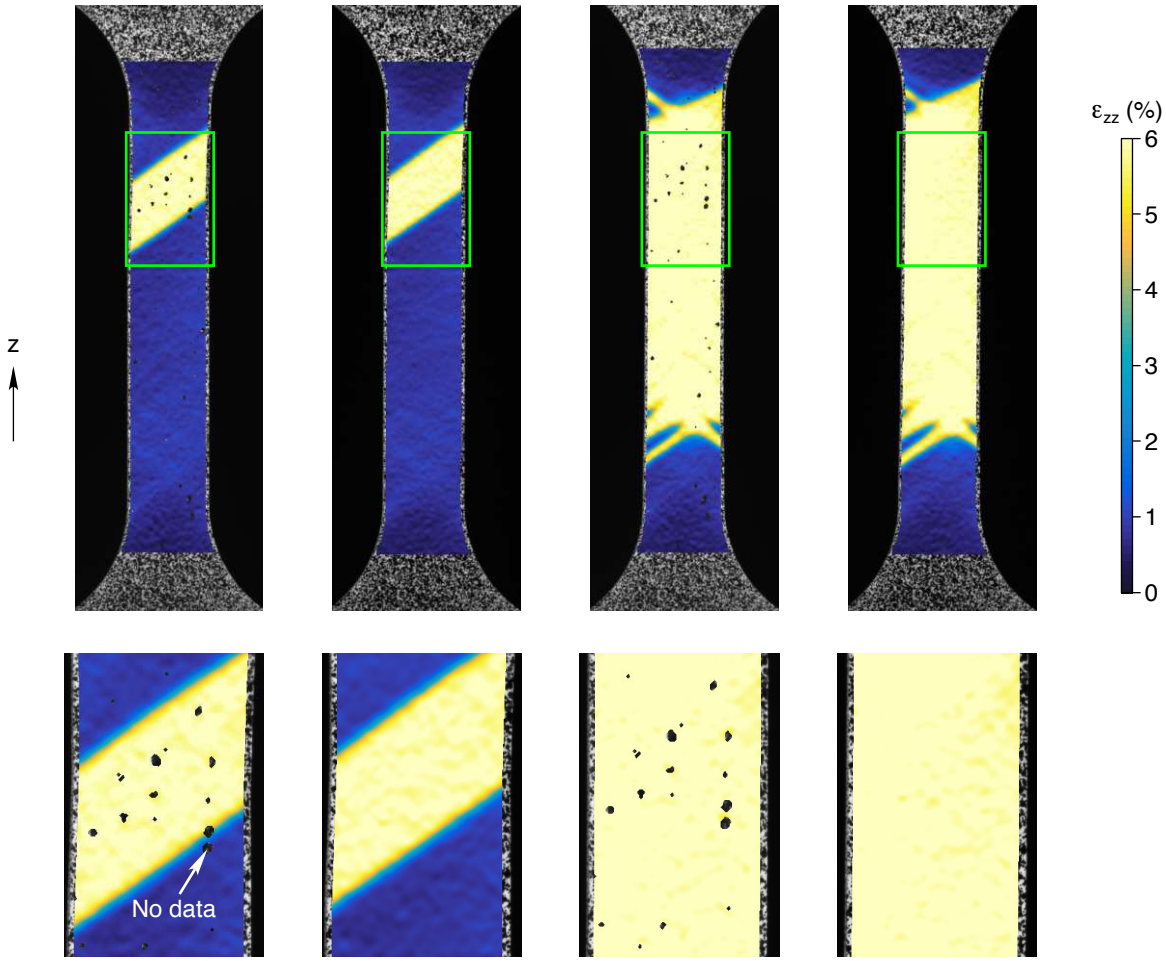

(a) Unpolarized ① (b) Cross-polarized ① (c) Unpolarized ② (d) Cross-polarized ②

Figure 15: With a decreased subset size of 15 px, the unpolarized images lost correlation for 1.3% of DIC points, especially in areas of large strains, while cross polarization lost none.

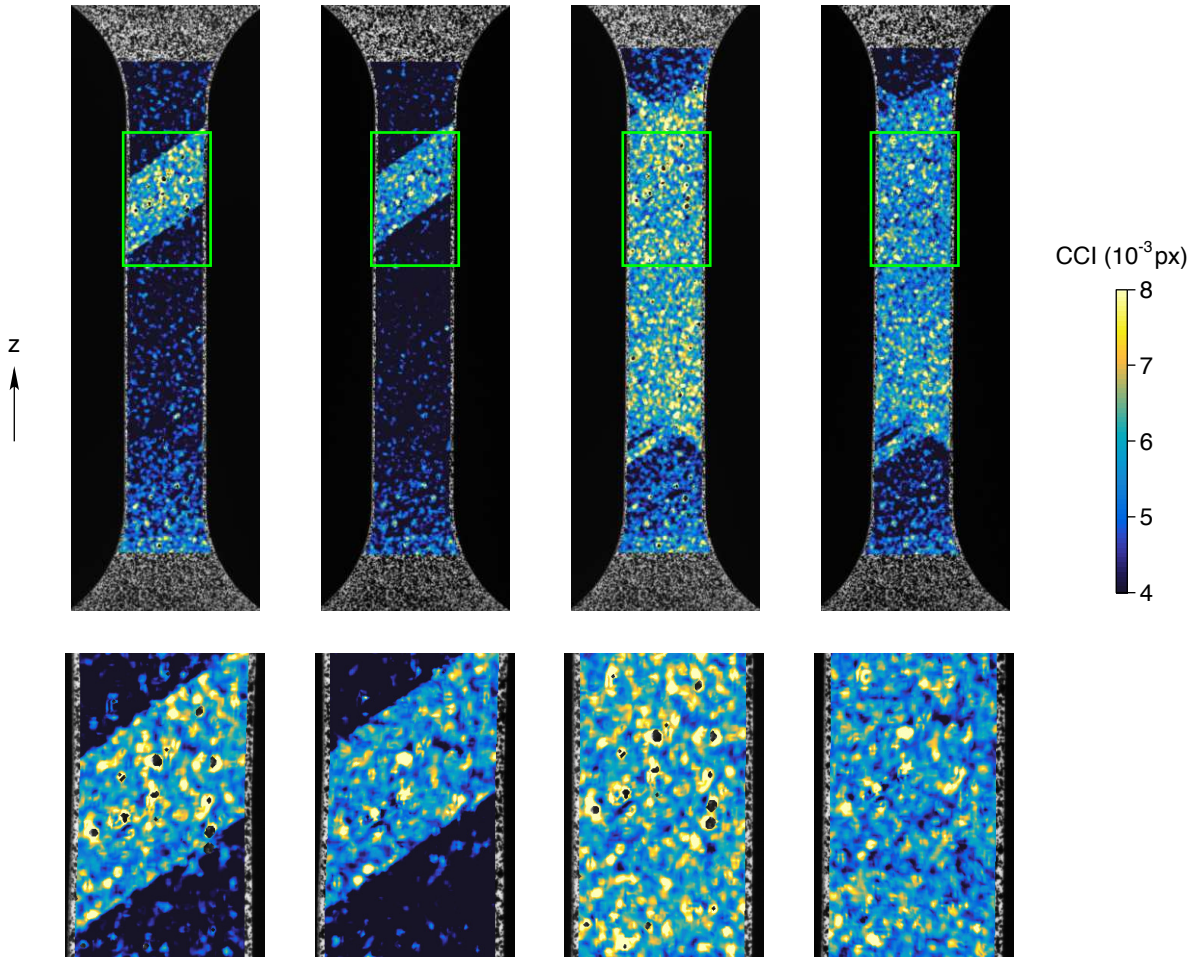

(a) Unpolarized ① (b) Cross-polarized ① (c) Unpolarized ② (d) Cross-polarized ②

Figure 16: With a decreased subset size of 15 px, cross polarization maintained better (smaller) correlation confidence intervals (CCI).

4 Discussion

As mentioned, cross polarization requires brighter lighting than without polarization because polarizing filters have transmission losses. According to the Law of Malus (Equation (3)), who discovered polarized light in 1808 [28], the transmission coefficient $T_{\max}$ of an ideal polarizer is $1/2$, or the average intensity through one period of rotation of the included angle (θ) between the polarizers, calculated as

$$I = I_0 \cos^2 \theta, \tag{3}$$

$$T_{\max} = \frac{I}{I_0} = \frac{1}{\pi} \int_{-\pi/2}^{\pi/2} \cos^2 \theta \, \mathrm{d}\theta = \frac{1}{2}, \tag{4}$$

where I_0 is the incident light intensity and I is the polarized light intensity. In practice, the transmission coefficient for cross polarizers is less than $1/2$. For example, the polarizing film for the light sources in this work had a transmission coefficient of 0.38.

It is not recommended to compensate for light transmission losses by using a larger aperture or a longer exposure time, instead of increasing the light intensity. A larger aperture (lower f-stop) would reduce the depth of field and lead to blurring for out-of-plane displacements. A longer exposure time could also lead to blurring if the specimen displaces too quickly [6] and would increase the effects of sensor noise, a potentially significant source of DIC error [12]. A concern with high-intensity lighting is the potential for heating of the ambient air (causing light distortion) and of temperature-sensitive specimens (such as the superelastic NiTi used here), but this can be avoided with high intensity LED light panels.

Another practical issue is the alignment of the polarizers, which require special care to orient orthogonally. If an imperfection angle θ_0 is introduced between cross polarizers, such that the included angle between the polarized directions is $\pi/2 \pm \theta_0$, the received light intensity $\tilde{I}$ (from imperfectly aligned polarizers) relative to the incident light intensity, extending from Equation (3), is

$$\frac{\tilde{I}}{I_0} = \cos^2 \left(\frac{\pi}{2} - \theta_0 \right). \tag{5}$$

This is plotted in Figure 17 to show the sensitivity of cross polarization to misalignment. As much as 3% of the light can still pass through the second polarizer with a misalignment of $\theta_0 = \pm 10^{\mathrm{o}}$. In this work, the angles of the light source polarizers were held equal and constant, and the angles of the camera lens polarizing filters were adjusted for maximum observable glare reduction during live imaging of the specimen.

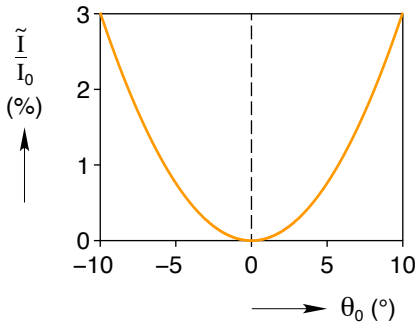

Figure 17: Polarizers should be carefully oriented orthogonally to maximize the benefits of cross polarization. The plot shows the relative "leakage" of light with imperfection angle θ_0.

5 Summary and Conclusions

Cross polarization is an effective method to prevent saturated pixels, increase image contrast, decrease DIC spatial smoothing, and preserve correlation robustness in optical 2-D and 3-D DIC. Cross polarization can reduce DIC error by attenuating glare that can saturate pixels and prohibit sub-pixel accuracy [6], and by increasing image contrast, which decreases both bias and random errors [12]. Cross polarization can also increase DIC spatial precision while preserving correlation robustness by decreasing the correlation confidence interval and allowing smaller subsets without exceeding correlation error thresholds. The only drawback we see to cross polarization is transmission losses from the polarizing filters, which can easily be counteracted with brighter lighting (although this is more difficult for high-speed imaging setups).

The differences between unpolarized and cross-polarized images were quantitatively evaluated with a rigid body translation experiment and a uniaxial NiTi tension test. For rigid body translations with four representative painted speckle patterns, cross polarization reduced 2-D DIC displacement measurement errors by at least 52% and as much as 61%. No significant changes in displacement measurement errors were observed for 3-D DIC, which already had very low errors for unpolarized images. Also for the rigid body translations, the correlation confidence interval for 3-D DIC was reduced with cross polarization by at least 6.3% and as much as 8.1%, and similar reductions in correlation confidence interval were observed for 2-D DIC.

Cross polarization increased the contrast and mean intensity gradient, two metrics that indicate speckle pattern and image quality. For example, with the uniaxial NiTi specimen, cross polarization increased the contrast by 11 grayscale counts and the mean intensity gradient by 7.4% (from 165.4 to 177.7 units of grayscale count gradient). These increases are significant since the pattern, lights, and cameras were considered optimum before the addition of cross polarization. The increased contrast allowed for very small subsets while maintaining more DIC data points within

correlation error thresholds: with 9×9 px subsets, the unpolarized images lost almost ten-fold more DIC data points than the cross-polarized images. The advantages of cross polarization would be even greater for samples with rounded features, such as tubes and rods, since specular reflections cannot be minimized with rounded samples simply by changing the positions of the lights and cameras.

For both the rigid body translation experiment and the uniaxial NiTi experiment, the unpolarized images always had instances of saturated pixels within the DIC area of interest, while none of the cross-polarized images had saturated pixels within the DIC area of interest. Preventing saturated pixels with cross polarization ensures the ability to compute displacements with sub-pixel accuracy.

Cross polarization requires brighter lighting (about 1.5× higher intensity) than without polarization, since polarizing filters introduce light transmission losses. Although the images would also be brighter with about two to three f-stops wider aperture or longer exposure time, brighter lighting is the best protocol with cross polarization because wider apertures decrease the depth of field and longer exposure times can dramatically increase CCD sensor noise and motion blur. Quality LED light panels are generally suitable because they provide bright, uniform light without specimen and ambient air heating.

Acknowledgments

We gratefully acknowledge financial support from the National Science Foundation (CAREER Award, CMMI-1251891) and the Department of Defense (NDSEG Fellowship).

References

[1] Peters W, Ranson W, Sutton M, Chu T, Anderson J (1983) Application of digital correlation methods to rigid body mechanics 22(6)

[2] Sutton M, Mingqi C, Peters W, Chao Y, McNeill S (1986) Application of an optimized digital correlation method to planar deformation analysis. Image and Vision Computing 4(3):143–150

[3] Bay B, Smith T, Fyhrie D, Saad M (1999) Digital volume correlation: Three-dimensional strain mapping using X-ray tomography. Experimental Mechanics 39(3):217–226

[4] Franck C, Hong S, Maskarinec S, Tirrell D, Ravichandran G (2007) Three-dimensional full-field measurements of large deformations in soft materials using confocal microscopy and digital volume correlation. Experimental Mechanics 47(3):427–438

[5] Reu P (2014) All about Speckles : Aliasing. Experimental Techniques 38:1–3

[6] Sutton M, Orteu J, Schreier H (2009) Image Correlation for Shape, Motion, and Deformation Measurements. Springer, New York, NY

[7] Reu P (2014) All about speckles : Speckle Size Measurement. Experimental Techniques 44(11):4–5

[8] Kammers A, Daly S (2013) Self-Assembled Nanoparticle Surface Patterning for Improved Digital Image Correlation in a Scanning Electron Microscope. Experimental Mechanics 53(8):1333–1341

[9] Reedlunn B, Daly S, Hector L Jr, Zavattieri P, Shaw J (2013) Tips and Tricks for Characterizing Shape Memory Alloy Wire: Part 5 – Full-field Strain Measurement by Digital Image Correlation. Experimental Techniques 37(3):62–78

[10] Reu P (2014) Speckles and their relationship to the digital camera. Experimental Techniques 38(4):1–2

[11] Hild F, Roux S (2012) Comparison of Local and Global Approaches to Digital Image Correlation. Experimental Mechanics 52(9):1503–1519

[12] Reu P (2015) All about Speckles: Contrast. Experimental Techniques 51(4):1–2

[13] Kwak J (2008) Digital Image Correlation (DIC) Methods for Small Scale Measurement. Master's thesis, Mechanical Engineering, State University of New York at Binghamton

[14] Adams A (1948), Basic Photo One: Camera and Lens

[15] Allphin W (1959), Primer of lamps and lighting

[16] Apolinar E, Rowe W (1980) Examination of human fingernail ridges by means of polarized light. Journal of Forensic Sciences 25(1):154–161

[17] Robertson A, Toumba K (1999) Cross-polarized photography in the study of enamel defects in dental paediatrics. Journal of Audiovisual Media in Medicine 22(2):63–70

[18] Kawara T, Obazawa H (1980) A New Method for Retroillumination Photography of Cataractous Lens Opacities. American Journal of Ophthalmology 90(2):186–189

[19] Anderson R (1991) Polarized light examination and photography of the skin. Archives of Dermatology 127(7):1000–1005

[20] Cooper M, Skaggs M, Reu P (2015) High-Speed Stereomicroscope Digital Image Correlation of Rupture Disc Behavior. Society of Experimental Mechanics 2015 Annual Conference

[21] LePage W, Shaw J, Daly S (2015) Thermomechanical Characterization of Shape Memory Alloy Mode I Fracture Behavior. Society of Experimental Mechanics 2015 Annual Conference

[22] Hanrahan P, Krueger W (1993) Reflection from layered surfaces due to subsurface scattering. In Proceedings of the 20th annual conference on Computer graphics and interactive techniques, 165–174, ACM

[23] Reu P (2015) Points on Paint. Experimental Techniques 39:1–2

[24] Pan B, Lu Z, Xie H (2010) Mean intensity gradient: An effective global parameter for quality assessment of the speckle patterns used in digital image correlation. Optics and Lasers in Engineering 48(4):469–477

[25] Prewitt J (1970) Object enhancement and extraction. Picture processing and Psychopictorics 10(1):15–19

[26] Kim K, Daly S (2010) Martensite Strain Memory in the Shape Memory Alloy Nickel-Titanium Under Mechanical Cycling. Experimental Mechanics 51(4):641–652

[27] Kim K, Daly S (2013) The effect of texture on stress-induced martensite formation in nickel–titanium. Smart Materials and Structures 22(7):075012

[28] Woodward C (1851), A familiar introduction to the study of polarized light